The 2022 WMO Technical Conference on Meteorological and Environmental Instruments and Methods of Observation (TECO-2022)

10-13 October 2022, Paris (France)

Adaptive diffraction corrections in solar radiometry, a prerequisite for the ISO 9060:2018 AA class

Suter, Markus[1]; Finsterle, Wolfgang[2];

[1] Davos Instruments AG, Davos Switzerland

[2] Physikalisch-Meteorlolgisches Observatorium Davos and World Radiation Centre (PMOD/WRC), Davos Switzerland

Corresponding author: Markus Suter, markus.suter@davos-instruments.ch

Abstract:

Diffraction effects in solar radiometry become more and more important once the target uncertainty goes below 0.1%. Diffraction effects occur at the apertures, and have an impact of roughly 0.1% and are strongly wavelength dependent. Therefore these effects can increase by up to 50% depending on the spectral conditions. It thus makes radiometers sensitive to the spectral distribution of the solar radiation, which is in turn is depending on atmospheric conditions.

The recently introduced AA class for pyrheliometers by ISO 9060:2018 calls for a "spectral error" lower than 100 ppm, which is impossible to reach without adaptive correction of the diffraction effect. Therefore it is necessary to actively correct for diffraction effects, depending of the actual spectrum.

Adaptive diffraction correction has first been studied for the Cryogenic Absolute Radiometer (CSAR), a future primary reference, that aims at very high absolute accuracy. In a second step, the study has been extended for PMO6/PMO8 radiometers.

In order to retrieve spectrally dependent diffraction corrections, corrections have been calculated for different modelled solar spectra based on an atmospheric model characterised by the key parameters: Solar zenith angle (SZA), integrated water vapour and aerosol optical depth (AOD). Using the atmosphere model, a spectrum and an associated diffraction correction is calculated for each parameter combination. Thus a multidimensional look-up table is generated, which allows to quickly retrieve a diffraction correction, based on the atmospheric conditions, that are simultaneously measured on many sites. Based on the look-up table error propagation can be studied, and the uncertainty of the diffraction correction can be estimated.

1. Introduction

High precision measurements of direct solar irradiance are typically performed with electrical substitution radiometers [WMO-CIMO (2018)]. These radiometers usually have a two aperture system, defining the field of view. Diffraction effects occur at the front aperture and influence the amount of light passing the second aperture.

The diffraction effect in solar radiometry has been previously discussed by many authors for example by Shirley (1998, 2005), Winkler (2013) and Suter (2015). Mostly the effect has been calculated for a standard spectrum and a fixed correction term has been applied to the measurements. While improving the accuracy of solar radiometers it has become evident to change to an adaptive diffraction.

The main motivation towards an adaptive diffraction correction are on the one hand the cryogenic CSAR reference radiometer [Winkler (2013)], and on the other hand the ISO9060:2018 that specifies a new AA-class for pyrheliometers. The CSAR is a cryogenic radiometer for outdoor use and a candidate for replacing the WRR standard [Finsterle (2016)]. It is described in detail by Winkler (2013). The ISO 9060 is a standard that classifies pyrheliometers and pyranometers. In its 2018 edition in introduces a new instrument class, the AA class that has not existed before. One of the challenges, in order to build an AA class radiometer is to overcome the spectral errors introduced by the diffraction effect

Considering the set of spectra given in ISO 9060:2018 (see Figure 1), it is found that widespread PMO6/PMO8 and HF type radiometers have an enhanced sensitivity (up to 400 – 500 ppm) compared to the standard conditions (spectrum G-173) for some of the spectra provided by ISO. As the AA class calls for a spectral error smaller that 100 ppm, it becomes clear that the diffraction effect must be treated adaptively in order to achieve the requirements.

Within this study the specific cases of the CSAR and the PMO6/PMO8 radiometers are assessed. The method however is universal and could be extended to other type of direct solar irradiance radiometers.

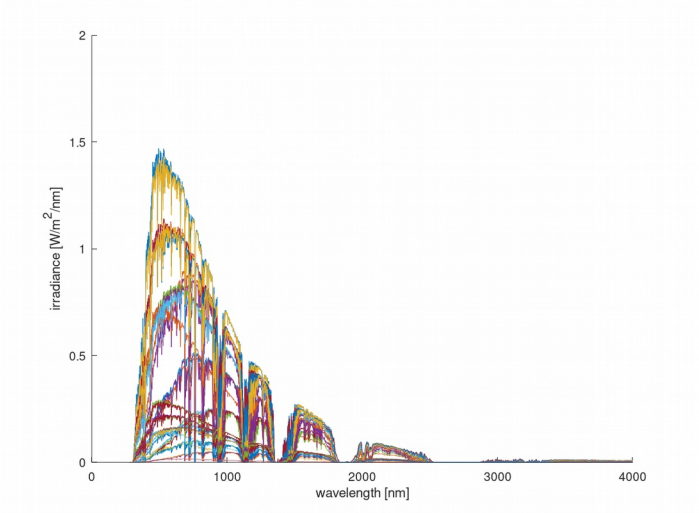

Figure 1: Solar reference spectra as provided by ISO 9060:2018

2. Methods

The basic approach to provide fast access to diffraction correction factors is to create a look-up table. This look-up table has several input parameters that describe the current atmospheric conditions, that can easily be measured.

In order to create this lookup table the diffraction effect as a function of wavelength needs to be known. In a second step a large amount of model spectra is generated, using different input parameters. For each spectrum a diffraction correction can be determined, by weighting the correction with each spectrum. In the case of CSAR that features an entrance window, also the characteristics of the window needs to be known. This workflow is illustrated in Figure 2. Using this multidimensional look-up table and linear interpolation, diffraction corrections can be accessed quickly without further model calculations.

The thus derived diffraction correction will be examined, and the sensitivity of each parameter is evaluated. Thus the necessary parameters can be identified.

Based on the input parameters, that are available on many sites, the diffraction correction can be quickly determined for each atmospheric situation.

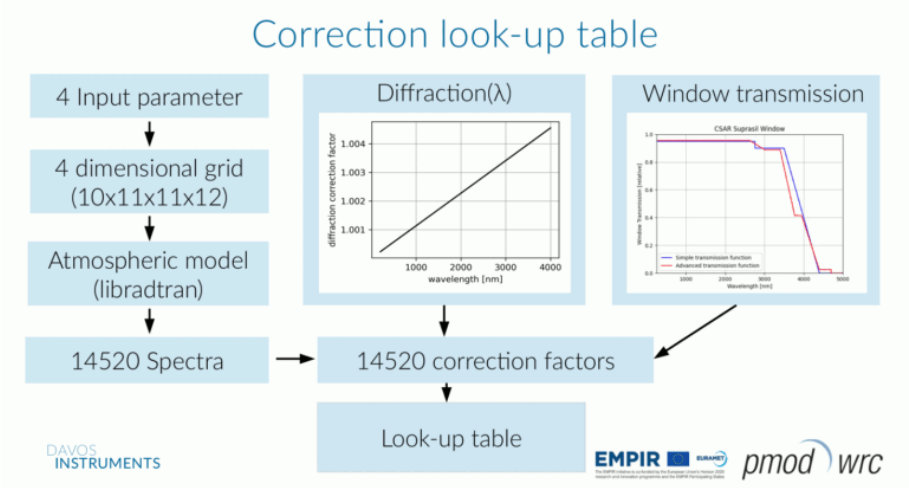

Figure 2: Building a look-up table, visualisation of the workflow

2.1. Diffraction Calculation

Diffraction effects have been studied since the 19th century, by Fraunhofer, Fresnel, Lommel and many more. Today, a broad literature is available on the topic. For the specific problem of the radiometer, we follow Suter (2015) and Shirley (1998, 2005).

At the radiometric two aperture system, diffraction occurs at the front aperture. A small portion of the light leaves the geometrical path. Thus the amount of solar radiation passing the second aperture and reaching the detector is reduced or enhanced, depending on the aperture layout.

The diffraction effect is wavelength dependent. The effect is larger for the longer wavelength and smaller for shorter wavelengths. As there are two basic aperture layouts, it needs to be distinguished between the CSAR layout and the typical WMO/ISO layout. The CSAR (and modern satellite based instruments) have the defining precision

aperture in front, and a view limiting aperture behind, just in front of the detector. (Figure 3, right). Traditional ground based radiometers (according to the CIMO guide [WMO 2018)] have the opposite geometry (Figure 3, left) This implies, that diffracted light enhances the signal in the traditional layout, while it lowers the received signal in the CSAR geometry.

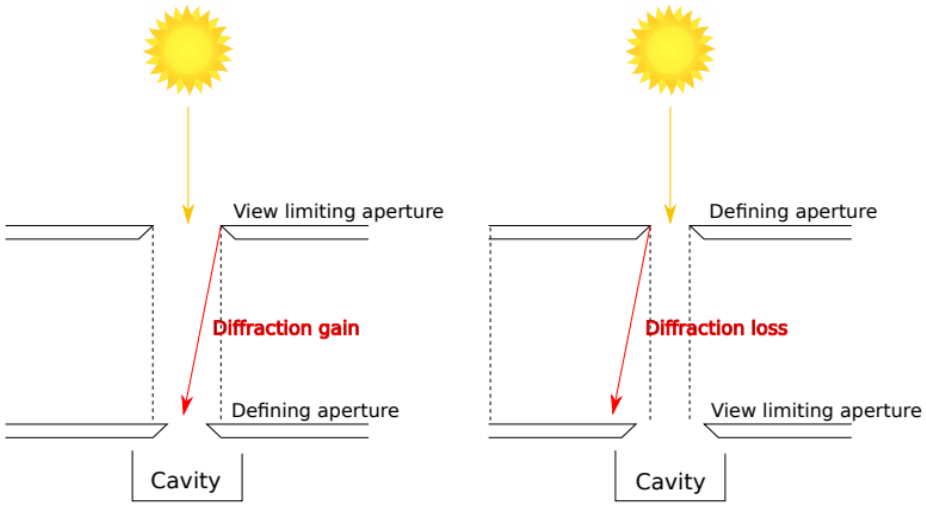

Figure 3: Schematics of the aperture geometry for the classic MWO-CIMO geometry (left) and CSAR right.

Table 1: Geometric Properties

	Radius Defining Aperture	Radius View Limiting Aperture	Distance between apertures
CSAR	2.5 mm	5 mm	104.0 mm
PMO8	2.5 mm	4.25 mm	95.4 mm

2.2. Spectral weighting and spectral modelling

After deriving the wavelength dependent correction, it needs to be weighted and integrated with the current solar spectrum. In order to receive the solar spectrum, based on basic atmospheric properties the atmospheric transfer model libRadtran [Emde et al. (2016)] is used. In the next sections, the input parameters of the model are described in detail.

2.3. Model Parameter

2.3.1. Solar Zenith Angle

The solar zenith angle is the most crucial parameter in the model. The zenith angle is variable with time, and defines the path length of the solar radiation through the atmosphere.

2.3.2. Integrated Water Vapour

Water molecules in the atmosphere are responsible for enhanced absorption of the radiation in the "red" part of the solar spectrum. Thus a high amount of water leads to a

decrease in diffraction, due to a reduced amount of radiation in the "red" part of the spectrum.

Integrated water vapour can be retrieved using band-filter radiometers [Nyeki, et al. (2005)] or GPS data [Wang et al. (2007)]

Figure 4 illustrates the seasonal variations of integrated water vapour for the Davos site [Suter (2015)].

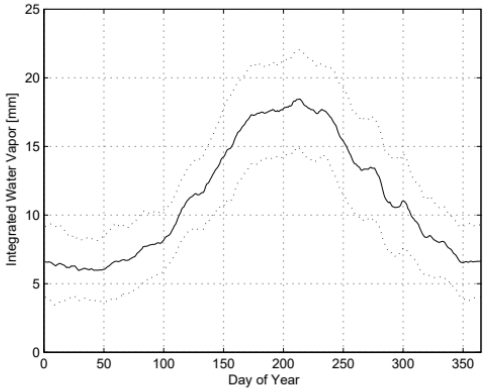

Figure 4: Seasonal variation of integrated water vapour for Davos with 1σ band showing the width of the distribution [Suter (2015)]

2.3.3. Aerosol Optical Depth (AOD)

A high aerosol load can have a significant impact on the solar spectrum. Aerosol impact on solar radiation is typically expressed by the aerosol optical depth (AOD). Within the model, AOD is parametrised as a function of wavelength, using the Angström formula:

$$\tau(\lambda) = \beta \lambda^{-\alpha}$$

where τ is the AOD and λ is the wavelength in μm

β can be interpreted as the aerosol optical depth at 1000nm. It describes the absorption in the atmosphere due to aerosols. α describes the wavelength dependence of the absorption due to aerosol. It can also be interpreted as approximation of the aerosol grain size distribution.

Aerosol Optical depth is retrieved with band-filter radiometers, as used in the GAW/PFR [Kazadzis et al (2005)] or the NASA/Aeronet network [Giles (2019)]. Major radiation stations worldwide are part of these networks.

2.3.4 Ozone

Ozone is responsible for absorbtion in the UV part of the solar spectrum. The total ozone column is mostly expressed in Dobson Units (DU). The ozone column cab for example be measured with a Brewer spectrophotometer [Kerr (2010)].

2.3.5. Window Transmission

While ground based ambient temperature reference radiometers do not have a window, the cryogenic CSAR radiometer has a window. The transmission of the suprasil window is thus also considered to adapt the spectrum.

The window transmission function has been provided by Fehlmann (2011). It has been approximated for the calculation of the diffraction corrections. Calculations for two different approximations (more detailed and less detailed) are carried out, in order to estimate an uncertainty contribution.

2.3.6 Uncertainties

The combined uncertainty associated with the derived correction factor is dependent on many parameters: Method based, uncertainty of the input parameters and absolute values of the input parameters. The look-up table and the corresponding software are able to calculate the error propagation, which can be used to estimate the uncertainty of each individual diffraction correction.

3. Results and discussion

After generating the look-up table for the diffraction correction, the results are compared to the diffraction correction derived by Winkler (2013) for the CSAR instrument. Then, the sensitivity of the correction to each input parameter has been investigated for different scenarios.

3.1. Comparison to the results from Winkler

The comparison between the numbers from Winkler (2013) and the results presented in this work for Davos conditions show a large discrepancy as the correction from Winkler (2013) is much more dependent on SZA. Looking deeper into the spectra used by Winkler (2013) and described by Fehlmann (2011) it seems that aerosol properties have not been given any attention. The described spectra have been derived using MODTRAN standard atmosphere properties, and the focus has clearly been on varying the solar zenith angle. Thus, most probably a significantly higher aerosol load has been supplied to the MODTRAN simulation by Fehlmann, compared to the LibRradtran simulation within this work. Furthermore, no effects of the CSAR window have been considered by Winkler (2013).

Supplying a higher AOD load to the current libRadtran model (AOD Angstrom α of 1.8 and β (aod) of 0.075, integrated water vapour) and neglecting the window, the values become more compatible with Winkler (2013). Example in Table 2. From this comparison it can be concluded, that there are some differences between the two calculation methods and this shall be treated as a systematic source of uncertainty.

Table 2: Comparison to Winkler (2013)

SZA	Correction Factor Winkler (2013)	Current sample calculation
0°	1.001071	1.001053
80°	1.001268	1.001271

3.2. Solar Zenith Angle

The solar zenith angle has a large impact on the diffraction correction. Varaition of the solar zenith angle between between 25° and 75° leads to variations of about 40 ppm for CSAR during a standard clear day in Davos (Figure 5, left). For the PMO6/PMO8 the

diffraction correction is larger and varies more (120 ppm) as a function of zenith angle. Figure 5 (right) shows a Davos standard scenario for PMO6/PMO8..

A smaller zenith angle, means a shorter path, and less absorption of blue light compared to the red light. A small zenith angle means less diffraction correction, whereas a larger zenith angle leads to a larger correction. When going to higher zenith angles, the effect increases rapidly as can be seen from Figure 5. Accurate diffraction correction become more difficult when going towards extreme zenith angles.

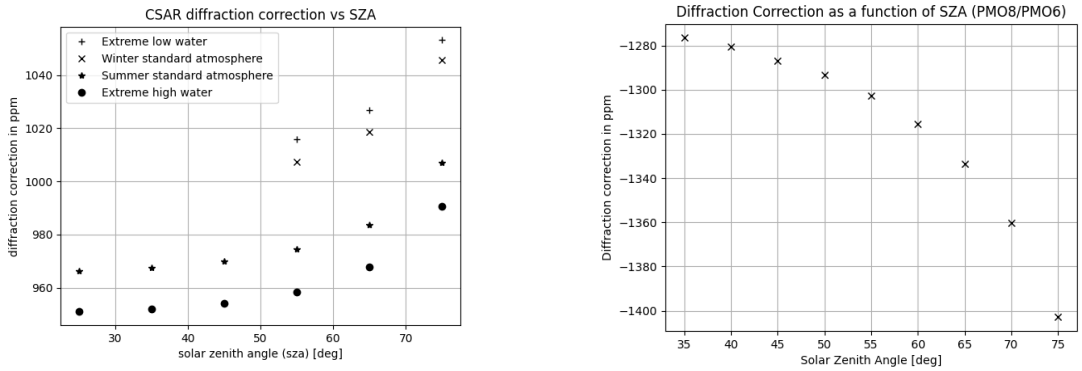

Figure 5: Diffraction correction versus solar zenith angle, for CSAR (left) and PMO6/PMO8 (right)

3.3. Integrated Water Vapour

Water vapour in the atmosphere absorbs in the red part of the solar spectrum, and thus lowers the diffraction effect. Figure xxx shows an example for CSAR at SZA 55°. It can be seen that the water vapour can significantly influence the diffraction correction.

3.4 Aerosol Optical Depth

Figure 7 shows the impact of the aerosol optical depth on the diffraction correction for CSAR for lower (Figure 7 left) and higher (Figure 8 right) aerosol concentration. At low AOD values (β) the change in the correction is only a few ppm, while at high AOD the additional contribution is considerable larger.

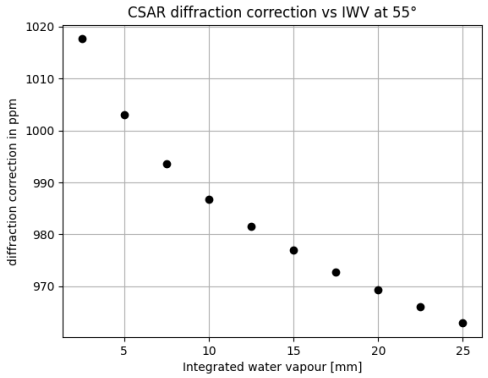

Figure 6: Diffraction corrections versus water vapour for CSAR

On a clear day (β<0.01) in Davos, aerosol has a very small impact on the diffraction effect. However for special conditions, for example a Saharan dust event, it is necessary

to account for AOD properties. When the aerosol load gets higher, the influence of the α parameter becomes relevant.

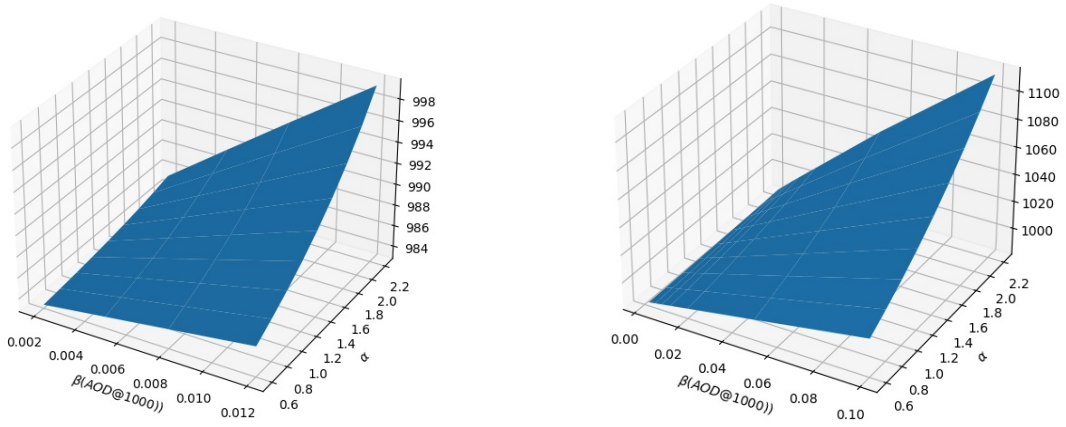

Figure 7: Diffraction Correction for CSAR as a function of AOD (α andβ) for low β (left) and high β on the right.

3.5. Ozone

The contribution of ozone has been investigated and found marginal. From the Davos time series (2006-2019, courtesy of Julian Gröbner PMOD/WRC) it is found that ozone concentration in Davos varies mostly between 250 and 400 DU. This leads maximal deviations in the diffraction correction of about 10 ppm at high a zenith angle of 80 degrees. For smaller zenith angles, the effect becomes mariginal. Figure 8 shows the impact of the ozone concentration for different zenith angles.

Therefore a fixed value of 315 Dobson units for Davos is implemented in the model. And a standard uncertainty of 40 DU is assumed. This results in a standard uncertainty component of the diffraction correction due to ozone of 3 ppm

3.6. Uncertainties

In Table 3 all the contributions to the combined uncertainty of the correction are listed, the numbers are for the CSAR. Uncertainty contributions can be separated into two categories: Uncertainties originating form the uncertainties of the model input parameters and uncertainties due to various effects that are independent form the model input.

The independent uncertainty contributions are mainly associated to the method itself and are in most cases not dominating the overall uncertainty. An interesting aspect is the influence of misalignment of the radiometer, that leads to a misalignment to of the rear aperture with respect to the front aperture. Thus the rear aperture does not cut out the centre of the diffraction pattern. This leads to a second order effect that will bias the measurement. For CSAR considering a misalignment of 0.1 deg this effect is only a few ppm, but rises quickly to 11 ppm at 0.2 deg and 26 ppm at 0.3 degrees of misalignment. For the PMO6/PMO8 these numbers are approximately doubled with 50 ppm at 0.3 degrees of misalignment. Thus a proper alignment is crucial to keep the uncertainties low.

Due to the capability of the look-up software to calculate error propagation, the influence of the uncertainty of input parameters, as well as the dependence of the combined

uncertainty to specific atmospheric conditions can be studied. Figure 8 shows the combined uncertainty for different solar zenith angles, considering the same uncertainties for the input parameters. It can be seen that for high zenith angles the combined uncertainty gets larger, considering the same absolute uncertainty of the input parameters. The parameters used are identical to the description in Table 3.

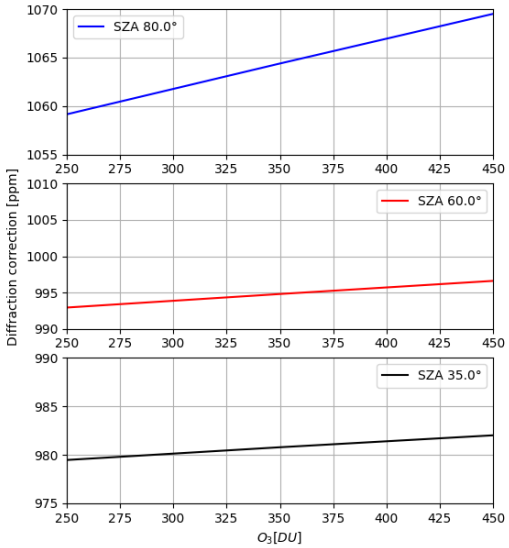

Figure 8: Diffraction correction for CSAR as a function of ozone concentration for three different zenith angles.

The uncertainty must be calculated considering the individual situation, data availability and quality. Nevertheless for illustration purposes an example situation (SZA = 55°, β =0.04, α=1.8 and iwv =10.5mm), is evaluated in Table 3. In this particular situation the contribution from the input parameters are approximately 30 ppm for CSAR and about 36 ppm for a PMO6/PMO8, see also Figure 9.

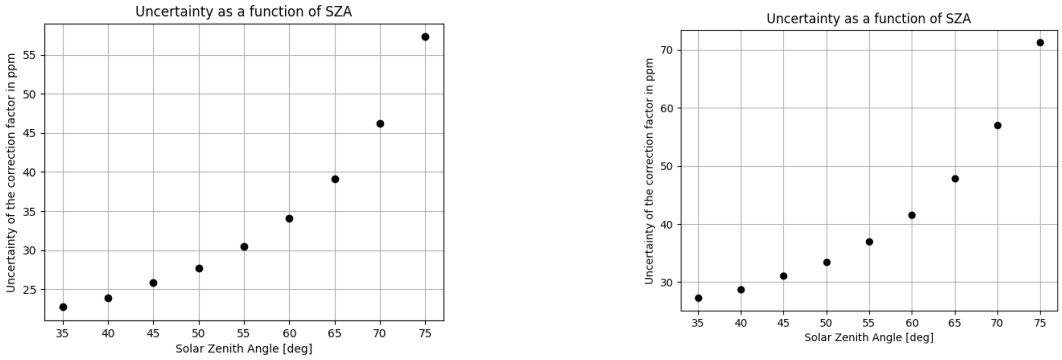

Figure 9: Combined standard uncertainties of the diffraction correction, based on the uncertainties of the input parameters as a function of solar zenith angles (left: CSAR, right: PMO6/8)

Table 3: Example of uncertainty budget for the diffraction correction factors.

Model parameter independent contributions	**Contribution Standard uncertainty**	**Comment**
Window Transmission	6 ppm	See section 2.2.5.
Difference between libradtran solvers	< 1 ppm	Different solvers have been compared. No significatnt difference could be found in the diffraction correction result.
Interpolation errors	< 5 ppm	Since the correction values are linear interpolations from the lookup table, there can be some interpolation errors, especially in extreme cases.
Sun-earth distance	< 1ppm	The effect of the varying sun-earth distance has been evaluated but found negligible.
Ozone	3 ppm	See section 3.5.
Systematic error of the calculation method	10 ppm	This value is derived from differences between Winkler 2013 and the current calculations. See also section 3.1.
Misalignment	4 ppm	If the two radiometer apertures are not properly aligned, the rear aperture will not capture the centre of the diffraction image. This secondary effect enhances the losses due to diffraction. A misalignment of 0.1 degree is considered in this example.
Combined	14 ppm	
Model parameter dependent contributions		
Matching of AOD Angstrom parameter to real situation.	up to 0.4 for alpha up to 0.03 for beta	These uncertainties are very much dependent on the actual situation. α uncertainty tends to be very high for low AOD situations. However the impact of an error in α gets small with low AOD. See also section 3.4. and Kazadzis et al (2005).
Integrated Water Vapour measurement	1 mm	approximately 1 mm, see also section 3.3.
Solar Zenith Angle	0.1°	Depends on the precision of the applied algorithm
Combined contribution of the model parameter for "Example Situation"	30 ppm	Example Situation: SZA = 55°, β =0.04, α=1.8 and IWV 10.5 mm relative uncertainties: Δsza=0.1°, Δiwv=1 mm, Δβ =0.03, Δα=0.2
Total combined uncertainty	33 ppm	In this example calculation the model parameter dependent contributions are dominating the uncertainty. This will be true for most real situations

4. Conclusions

The presented approach allows to quickly assess diffraction corrections based on widely available atmospheric parameters. This allows for adaptive and even real time corrections of high precision solar irradiance measurements, as well as quick uncertainty assessment.

Four parameters have been identified to be relevant for the determination of the diffraction correction. These are the solar zenith angle, the integrated water vapour and the aerosol optical depth, expressed by α and β parameters.

The uncertainties under reasonable conditions have been estimated to about 65 ppm (k=2) for CSAR. However the combined uncertainty is heavily dependent on the atmospheric conditions, and the accuracy of the atmospheric parameters and must always be assessed individually. The uncertainty contribution of a possible misalignment that can enhance the diffraction effect, has been identified and proper alignment of the radiometer has been found crucial. For CSAR , that is primarily located at the Davos site, the proposed method will help to further improve the accuracy.

The presented approach has been applied to PMO6/PMO8 radiometers, and can be extended of other type of pyrheliometers. Standard uncertainties of the corrections for typical Davos conditions are in range well bellow 100 ppm that is the target uncertainty for spectral errors for the ISO9060:2018 AA class. However the spectra provided by ISO9060:2018 have air masses up to 5, that corresponds to approximately 78 degrees solar zenith angle, and much higher aerosol loads which leads to higher uncertainties than presented in this work. It thus remains to prove if and how AA class criteria can be met for all applicable situations.

5. References

Emde, C., Buras-Schnell, R., Kylling, A., Mayer, B., Gasteiger, J., Hamann, U., Kylling, J., Richter, B., Pause, C., Dowling, T. and Bugliaro, L. The libradtran software package for radiative transfer calculations (version 2.0.1). Geoscientific Model Development, 9(5):1647-1672, 2016.

Fehlmann, A. Metrology of Solar Irradiance, PhD thesis, University of Zurich, 2011.

Finsterle, W. International Pyrheliometer Comparison (IPC-XII), Final Report. WMO IOM Report No. 124, World Meteorological Organization, Genève CH, 2016

Giles, D. M., Sinyuk, A., Sorokin, M. G., Schafer, J. S., Smirnov, A., Slutsker, I., Eck, T. F., Holben, B. N., Lewis, J. R., Campbell, J. R., Welton, E. J., Korkin, S. V., and Lyapustin, A. I. Advancements in the Aerosol Robotic Network (AERONET) Version 3 database – automated near-real-time quality control algorithm with improved cloud screening for Sun photometer aerosol optical depth (AOD) measurements, Atmos. Meas. Tech., 12, 169–209, 2019.

Kazadzis, S., Kouremeti, N., Nyeki, S., Gröbner, J., and Wehrli, C. The World Optical Depth Research and Calibration Center (WORCC) quality assurance and quality control of GAW-PFR AOD measurements, Geosci. Instrum. Method. Data Syst., 7, 39–53, 2018.

Kerr, J.B. The Brewer Spectrophotometer. In: Gao, W., Slusser, J.R., Schmoldt, D.L. (eds) UV Radiation in Global Climate Change. Springer, Berlin, Heidelberg, 2010

Nyeki, S., Vuilleumier, L., Morland, J., Bokoye, A., Viatte, P., Mätzler, C. and Kämpfer, N. A 10-year integrated atmospheric water vapor record using precision filter radiometers at two high-alpine sites, Geophys. Res. Lett., 32, L23803, 2005.

Shirley, E.L. 9. Diffraction Effects in Radiometry. In Optical Radiometry Series: Experimental Methods in the Physical Sciences, volume 41, pages 409-415. Elsevier, 2005.

Shirley, E.L. Revised Formulas for Diffraction Effects with point and Extended Sources. Applied Optics, 37:6581-6590, 1998.

Suter, M. Advances in Solar Radiometry, PhD thesis, University of Zurich, 2015.

Wang, J., Zhang, L., Dai, A., Van Hove, T., and Van Baelen, J. A near-global, 2-hourly dataset of atmospheric precipitable water from ground-based GPS measurements, J. Geophys. Res., 112, D11107, 2007.

Winkler, R. Cryogenic Solar Absolute Radiometer - a Potential SI Standard for Solar Irradiance. PhD thesis, University College London UK, 2013.

ISO 9060:2018, Solar energy — Specification and classification of instruments for measuring hemispherical solar and direct solar radiation, 2018.

WMO-CIMO, Comission for Instruments and Methods of Observation (CIMO), Guide to Instruments and Methods of Observation (WMO-No. 8), Wolrd Meteorological Organisation, Genève, CH, 2018.